Water Research 253 (2024) 121260

Contents lists available at ScienceDirect

Water Research

journal homepage: www.elsevier.com/locate/watres

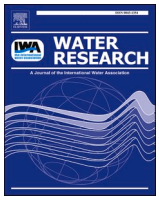

Photo-production of excited triplet-state of dissolved organic matters in inland freshwater and coastal seawater

Zhongyu Guo [a], Tingting Wang [b], Hidetaka Ichiyanagi [c], Mohamed Ateia [d], Guo Chen [a], Jieqiong Wang [e], Manabu Fujii [a], Kaichii En [f], Tiansheng Li [g], Rumi Sohrin [h], Chihiro Yoshimura [a,*]

[a] Department of Civil and Environmental Engineering, Tokyo Institute of Technology, Meguro-Ku, Tokyo, 152-8552, Japan
[b] Graduate School of Science, Nagoya University, Furo-Cho, Chikusa-Ku, Nagoya, 464-8602, Japan
[c] Water Resources Environment Center, Tokyo, 102-0083, Japan
[d] Department of Chemical and Biomolecular Engineering, Rice University, Houston, TX, USA
[e] College of Environmental Science and Engineering, North China Electric Power University, Beijing 102206, China
[f] Department of Chemistry, School of Science, Tokai University, Kitakaname, Hiratsuka-shi, Kanagawa 259-1292, Japan
[g] Laboratory for Zero-Carbon Energy, Institute of Innovative Research, Tokyo Institute of Technology, Meguro-Ku, Tokyo, 152-8552, Japan
[h] Institute of Geosciences, Shizuoka University, 836 Oya, Suruga, Shizuoka, 422-8529, Japan

ARTICLE INFO

Keywords:
High-energy triplets
Modeling
Optical property
Photochemistry
Quantum yield coefficient

ABSTRACT

The excited triplet-state of dissolved organic matter (^{3}DOM*) is a major reactive intermediate in sunlit waters. Its quantum yield is important in understanding the fate of organic micropollutants. The degradation efficiency of its chemical probe, 2,4,6-trimeythlphenol (f_{TMP}), is generally used as a proxy of the quantum yield. However, f_{TMP} has been described and modelled only for freshwater systems. Therefore, this study quantified f_{TMP} in inland freshwater and coastal seawater sampled in Japan by conducting steady-state photochemical experiments. Optical properties of water were then used to model f_{TMP}. Results indicated that the inland freshwater DOM originated mainly from terrestrial sources, while the coastal seawater DOM were microbial-dominated. On average, inland freshwater exhibited lower f_{TMP} (61.2 M^{-1}) than coastal seawater (79.7 M^{-1}) and the coastal seawater exhibited significant variations in the proportion of high-energy ^{3}DOM* (> 250 kJ/mol). In addition, E_2:E_3 (ratio of absorbance at 254 to 365 nm) was positively correlated with f_{TMP} of inland freshwater, coastal seawater, and the overall dataset. Catchment conditions such as forest coverage also influenced the production of ^{3}DOM* and high-energy ^{3}DOM* in inland freshwater. Furthermore, the developed models estimated f_{TMP} based on the optical properties of both freshwater and seawater, providing valuable insights about ^{3}DOM* photochemistry in the aquatic environment.

1. Introduction

Dissolved organic matter (DOM) is ubiquitous in the aquatic environment and plays a crucial role in global carbon cycling and other biogeochemical processes (Kieber et al., 1989). As DOM is generally capable of absorbing sunlight, DOM actively participates in numerous photochemical reactions. Upon absorption of light, chromophores within DOM become excited and undergo intersystem crossing, resulting in its triplet-state (^{3}DOM*) (McNeill and Canonica, 2016). It can directly react with many organic micropollutants, ultimately leading to their degradation (Lian et al., 2020; McNeill and Canonica, 2016). Particularly, high-energy ^{3}DOM* (Hi-^{3}DOM*, triplet energy over 250 kJ/mol), plays a critical role in the degradation of organic micropollutants (via both energy transfer and oxidation reactions) due to its high reactivity (Guo et al., 2021; McNeill and Canonica, 2016; Wang et al., 2020; Zepp et al., 1985). Meanwhile, ^{3}DOM* can serve as a precursor for several other reactive intermediates (RIs), such as singlet oxygen ($^1O_2$) and hydroxyl radical, all of which are involved in the degradation of organic micropollutants (Boreen et al., 2003; Guo et al., 2023a; Vione et al., 2014; Yan and Song, 2014), inactivation of pathogens (Wenk et al., 2019), and global carbon cycling (Mopper and Kieber, 2000). Thus, it is necessary to investigate the photo-production of

* Corresponding author.
E-mail address: yoshimura.c.aa@m.titech.ac.jp (C. Yoshimura).

https://doi.org/10.1016/j.watres.2024.121260
Received 18 October 2023; Received in revised form 27 December 2023; Accepted 3 February 2024
Available online 8 February 2024

^{3}DOM* in the aquatic environment to comprehensively understand ^{3}DOM*-induced biogeochemical processes.

The apparent quantum yield coefficient for the photo-production of ^{3}DOM* describes the efficiency of environmental water in producing ^{3}DOM* and can be used to estimate its steady-state concentration under sunlit condition (Carena et al., 2023; Vione, 2020). This is commonly quantified using the quantum yield coefficient of the chemical probe, 2, 4,6-trimethylphenol (TMP), for ^{3}DOM* (denoted as f_{TMP}). f_{TMP} varies among water bodies, mainly depending on the quality of the DOM (Wang et al., 2019) and the coexisting components that act as ^{3}DOM* quenchers. Previous studies have reported that f_{TMP} of coastal seawater DOM is higher than that of inland freshwater DOM (Chen et al., 2019; Guo et al., 2021; Wang et al., 2019), which could be attributed to differences in their composition and structure. DOM in inland freshwater such as rivers and lakes, in case of no major pollution, typically consists of lignin and tannin derivates from higher plants in their catchments (McCabe and Arnold, 2017; McKnight et al., 2001). In contrast, coastal seawater DOM generally contains polysaccharides, acetate, and lipids in certain proportions with abundant carboxyl-rich alicyclic molecules from cellular excretions of phytoplankton, algal, bacterial and so on (Aluwihare et al., 1997; Benner et al., 1992; Dittmar and Stubbins, 2014; Seidel et al., 2022; Thornton, 2014). Such distinct chemical structures determine the photo-reactivity of DOM (Osburn et al., 2011; Osburn and Bianchi, 2016; Wang et al., 2019). However, the relationship between f_{TMP} and bulk DOM properties has been described only for freshwater systems; thus, the major DOM property responsible for the global variability of f_{TMP}, including both freshwater and seawater systems, remains uncertain.

Consequently, similar progress and limitations can be seen in the model development for estimating f_{TMP}. Optical properties of DOM allow us to accurately estimate f_{TMP}, which may provide insights into the mechanism of the photo-production of ^{3}DOM* and reduce the cost of experimental determination of f_{TMP}. This has advantages for the management of organic micropollutants. To date, almost all models for f_{TMP} have been developed with a focus on freshwater systems, such as rivers, lakes, wetlands, and wastewater effluents (Berg et al., 2023; Chen et al., 2020; McCabe and Arnold, 2018, 2016; McKay et al., 2017; Wang et al., 2021; Wasswa et al., 2020). However, such an attempt has not been reported for coastal seawater, even though seawater possesses distinct DOM properties from inland freshwater. Recently, a machine-learning model was applied to f_{TMP} of both inland freshwater and coastal seawater, although over 99 % of these data (i.e., f_{TMP} and bulk water properties) was derived from inland freshwater (Liao et al., 2023).

This limits our understanding and capacity to estimate the photo-production of ^{3}DOM* in aquatic environments, given that pollutants have been detected in both freshwater and seawater. Therefore, a comprehensive investigation, including both inland freshwater and coastal seawater, is of practical significance for gaining deep insights into the relevant chemical structure of DOM and water properties for modeling f_{TMP}. Development of f_{TMP} estimation models that work across various aquatic environments will also help us accurately estimate the steady-state concentration of ^{3}DOM* and the resulting degradation of organic micropollutants in a water environment. Furthermore, the ^{3}DOM*-induced degradation processes could become increasingly important for pollutant removal as the deoxygenation of natural waters due to climate change continues (Zhi et al., 2023) because less ^{3}DOM* can be quenched by oxygen than before (Vione et al., 2023). Thus, characterization of ^{3}DOM* in terms of reactivity (i.e., Hi-^{3}DOM*) will help us gain insights into the disparate reactivities of ^{3}DOM* from different waters (Erickson et al., 2018; Wang et al., 2019).

Thus, this study aimed to understand the bulk water properties that determine the photo-production of ^{3}DOM* and Hi-^{3}DOM* by covering inland freshwater and coastal seawater. To achieve this, we sampled inland freshwater and coastal seawater in and around Japan and quantified and statistically modelled their f_{TMP} as well as the contribution of Hi-^{3}DOM*. Inland freshwater was collected in dam reservoirs as representatives of freshwater systems because dam reservoirs show characteristics of both rivers and lakes, two major freshwater bodies, in terms of DOM (Guo et al., 2023b).

2. Materials and methods

2.1. Chemicals and reagents

Information on the chemicals and reagents is in Text S1.

2.2. Water sampling and characterization

For inland freshwater, sampling and characterization of 50 reservoirs (F1–F50) (Fig. 1) have been detailed previously (Guo et al., 2023b). The reservoirs vary in different aspects such as depth, elevation, latitude, and so on (Table S1). Their catchments encompass a wide range of areas, populations, and particularly land cover types (Table S2), which were quantified using the ArcMap software as detailed in Text S2. In addition, 30 coastal seawater samples (S1–S30) were collected from the nearshore areas around the major islands of Japan from November 2022 to May 2023. The nearshore surface water of eight lake/pond samples (L1–L8) were also collected mainly in November of 2022 (Fig. 1 and Table S3). All the water samples were filtered with 0.45 μm polytetrafluoroethylene membrane filters (Omnipore, Merck Millipore Ltd., Ireland) immediately after arrival in the laboratory and stored at 4 °C before f_{TMP} determination and water quality analysis.

Bulk water properties were determined and used to develop f_{TMP} estimation models. The determined properties included pH, dissolved organic carbon (DOC), inorganic ions, salinity, conductivity, and optical data namely, UV–vis spectra and excitation-emission matrices (EEMs) (details in Text S3). The UV–vis spectra and EEMs were used to calculate optical indicators of spectral slope coefficients ($S_{275-295}$, $S_{350-400}$, and $S_{300-600}$), spectral slope ratio of $S_{275-295}$ to $S_{350-400}$ (S_R) (Helms et al., 2008), biological index (BIX) (Huguet et al., 2009), humification index (HIX) (Ohno, 2002; Zsolnay et al., 1999), and peak intensities *b, t, a, m*, and *c* (Coble, 1996; Huguet et al., 2009), fluorescence index (FI) (McKnight et al., 2001), absorption coefficients at 254 and 300 nm (a_{254} and a_{300}), specific UV absorbance at 254 nm ($SUVA_{254}$) (Weishaar et al., 2003), and E_2:E_3.

2.3. Determination of f_{TMP}

A photo-reactor (Helios.Xe, Koike Precision Instruments, Japan) equipped with a 300 W xenon lamp surrounded by 280 nm cut-off filters was used for photochemical experiments, as detailed by Guo et al. (2023b). The temperature was maintained at 20 °C using a water bath and the total irradiance from 280 to 400 nm was determined to be 1.71×10^{-5} Einstein L^{-1} s^{-1} using *p*-nitroanisole/pyridine (Laszakovits et al., 2017) (Figure S1). The pH was adjusted to 8.0 ± 0.1, which is the average of reservoir and coastal seawater samples.

50 μM of TMP was used to probe ^{3}DOM* (De Laurentiis et al., 2013; Rosario-Ortiz and Canonica, 2016). At 50 μM of TMP or less, the quenching rate of ^{3}DOM* was not significantly changed as dissolved oxygen is still the major quencher for ^{3}DOM* (Text S4). TMP has been previously used as a ^{3}DOM* probe for high-saline DOM solutions as well (Glover and Rosario-Ortiz, 2013) and the possible interference from the produced Br radicals was confirmed to be minor under the presented experimental conditions (detailed in Text S5). f_{TMP} was calculated instead of quantum yield for the production of ^{3}DOM* because of the diverse reactivities of ^{3}DOM* from different sources (Erickson et al., 2018). f_{TMP} was calculated using the following equations (Eqs. (1) and (2)).

$$f_{TMP} = k_{TMP}/R_{abs} \quad (1)$$

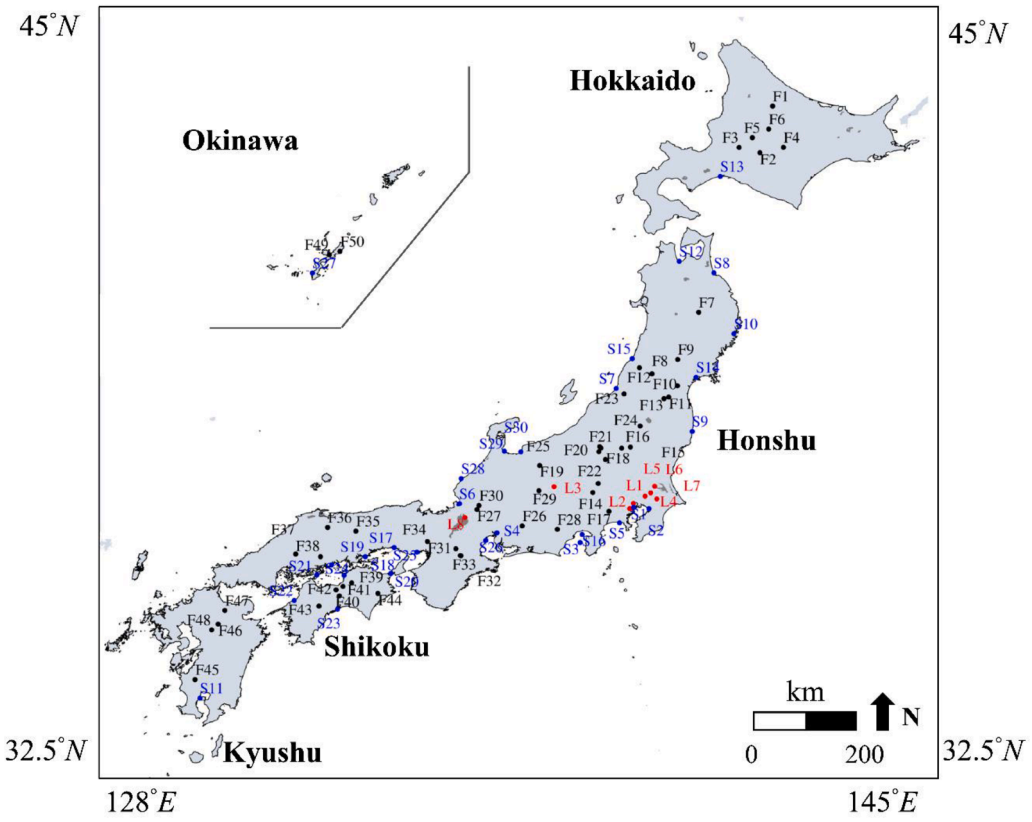

Fig. 1. Sampling map of the reservoir (F1–F50 in black), coastal seawater (S1–S30 in blue), and lake/pond samples (L1–L8 in red).

$$R_{abs} = \frac{1}{l}\sum_{\lambda} I_{0,\lambda}\left(1 - 10^{-\alpha_\lambda l}\right)\Delta_\lambda \quad (2)$$

where k_{TMP} (s^{-1}) is the first-order degradation rate constant of TMP, which was determined by high-performance liquid chromatography (Text S6); R_{abs} is the light absorption rate from 280 to 400 nm using Eq. 2; l is the optical path length of the tube; $I_{0,\lambda}$ is the absolute spectral irradiance of the incident light (in (mol photons) s^{-1} nm^{-1} cm^{-2}); and α_λ is the decadic absorption coefficient of the reservoir sample (in cm^{-1}).

The proportion of Hi-^{3}DOM* was investigated by adding 1 mM sorbic alcohol (SA) to quench Hi-^{3}DOM* in the solutions (Zhou et al., 2019). The shift of f_{TMP} ($f_{Hi\text{-}TMP}$) was attributed to the quenching of Hi-^{3}DOM*.

$$f_{Hi-TMP} = (k_{TMP} - k_{TMP-SA})/R_{abs} \quad (3)$$

where $k_{TMP\text{-}SA}$ is the first-order degradation rate constant of TMP after the addition of 1 mM SA.

2.4. Data analysis and empirical models

Pearson's correlation analysis was applied to f_{TMP}, bulk water properties, and catchment characteristics, and significantly correlated properties ($p < 0.05$) were used to develop simple linear regression (SLR) models. Then, orthogonal partial least squares (OPLS) regression (*ropls* package) (Thévenot et al., 2015) validated by cross-validation, was used to identify the most influential bulk water properties as predictors for developing stepwise multiple linear regression (MLR) models (forward selection with a criterion of $p < 0.1$). These regressions were performed using the R programming (R 4.2.3). Furthermore, we employed the random forest (RF) method, which can capture the non-linear patterns in the dataset and is largely immune to collinearity among predicators (Lindner et al., 2022), to develop the f_{TMP} estimation model for three datasets: freshwater, coastal seawater, and their combined dataset. For each of them, the dataset was split into training set (80 %) and testing set (20 %) for fitting and evaluating models by using *sklearn's RandomForestRegressor* function in Python package (detailed in Text S7). The performance of all models was evaluated using the coefficient of determination (r^2) and root mean square error (RMSE). The f_{TMP} of the lake/pond and the reference natural organic matter (NOM) were employed to test the performance of the developed SLR, MLR, and RF models.

3. Results and discussion

3.1. Bulk water property of freshwater and coastal seawater

The concentrations of NO_3^-/NO_2^- in coastal seawater samples were under detection limit of the applied method (< 0.01 mg L^{-1}, Table S4) and the highest concentrations of NO_3^- and NO_2^- were 3.98 mg L^{-1} and 0.40 mg L^{-1} in freshwater samples (Table S5). The DOC ranged from 0.46 mgC L^{-1} to 2.10 mgC L^{-1} in freshwater samples and 0.71 mgC L^{-1} to 1.47 mgC L^{-1} in coastal seawater samples, with an average value of about 1 mgC L^{-1} for both. Thus, the light absorption by NO_2^- and NO_3^- was marginal (detailed in Text S8) and DOM was the major light-absorbing component. DOC, pH (≈ 8), $S_{350-400}$, $S_{300-600}$, and FI showed no significant difference between inland freshwater and coastal seawater samples (Fig. 2 and Tables S3, S6 and S7). In contrast, the averages of $SUVA_{254}$, a_{300}, and HIX of freshwater samples were significantly higher than coastal seawater samples (Fig. 2), indicating a higher degree of aromaticity and hydrophobic organic acids ($SUVA_{254}$ and a_{300}), and a longer period of humification (HIX) compared to DOM from coastal seawater (D'Andrilli et al., 2022; Spencer et al., 2012). Meanwhile, the averages of E_2:E_3, $S_{275-295}$, and BIX of freshwater samples were significantly lower than coastal seawater samples, suggesting the dominance of high-molecular-weight components in freshwater DOM compared to the coastal seawater DOM (Helms et al., 2008; Peuravuori and Pihlaja, 1997). Furthermore, BIX of the coastal seawater DOM was

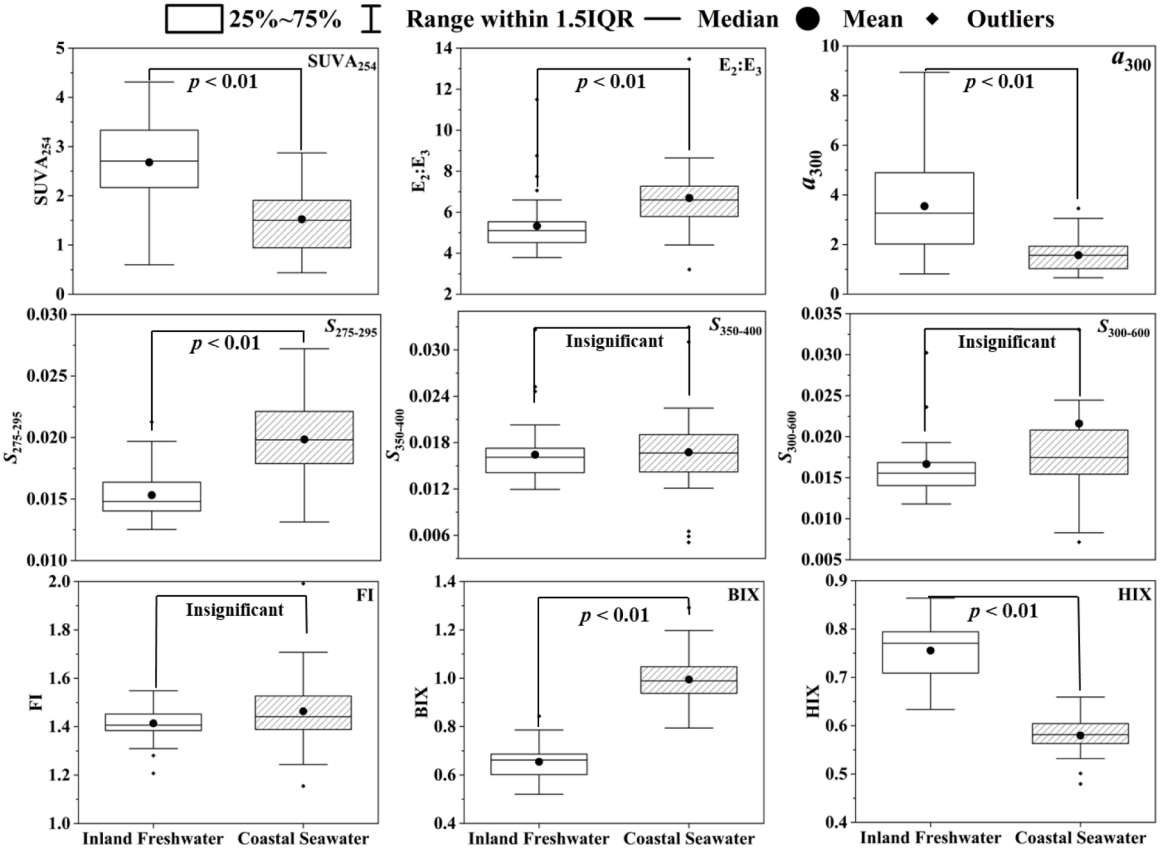

Fig. 2. Main bulk water property of inland freshwater ($n = 50$) and coastal seawater samples ($n = 30$). IQR: interquartile range. Significant differences between two sample sets were analyzed by *t*-test with significance level of 0.05.

close to unity, demonstrating that the seawater DOM are predominantly microbial, whereas a mean of 0.65 for BIX of the freshwater DOM indicates a terrestrial source (Huguet et al., 2009). In summary, the freshwater DOM originated mainly from terrestrial sources, while the coastal seawater DOM were microbial-dominated. Seawater DOM exhibited lower light absorption ability, contained a relatively higher abundance of low-molecular-weight components, and underwent less humification than freshwater DOM.

3.2. Quantum yield coefficient of ^{3}DOM* (f_{TMP})

TMP degradation followed pseudo-first-order kinetics ($r^2 > 0.96, p < 0.05$) (Figure S2). f_{TMP} of the referenced Suwannee River Fulvic acid (SRFA) and Suwannee River natural organic matter (SRNOM) fell within the previously reported range (Table S8), indicating the reliable determination of f_{TMP} in our experiments. f_{TMP} of freshwater samples ranged from 31.3 M^{-1} of Sameura dam (F40) to 168 M^{-1} of Shimokubo dam (F22) with an average of 61.2 M^{-1} (Fig. 3a and Table S9). This average was significantly lower ($p < 0.01$) than that of coastal seawater samples (79.7 M^{-1}), which ranged from 27.0 M^{-1} of Mutsu Bay (S12) to 176 M^{-1} of Wakasa Bay (S6). This difference can be caused by the different average DOM properties of these two types of water (Section 3.1).

Most of the f_{TMP} (> 70 %) occurred between 30 M^{-1} and 65 M^{-1} for freshwater samples, whereas f_{TMP} varied mainly (> 76 %) between 60 M^{-1} and 100 M^{-1} for coastal seawater samples, inferring the presence of different major DOM components responsible for the photo-production of ^{3}DOM*. This difference in ^{3}DOM* precursors could be resulted from the tendency of the less aromatic and more branched aliphatic structures in seawater DOM than in freshwater DOM (Wang et al., 2019). Meanwhile, they showed a certain overlap in f_{TMP} (i.e., 60 M^{-1} to 70 M^{-1}), indicating either similar chemical components of DOM in terms of ^{3}DOM* production or different quenching effects of ^{3}DOM*, which resulted in a similar f_{TMP} (Wenk and Canonica, 2012). The different concentration levels of coexisting inorganic salts might be another factor because halide ions and TMP might competitively consume ^{3}DOM* (Parker and Mitch, 2016).

The average f_{TMP} of the coastal seawater samples was higher than that of the freshwater samples, whereas it was significantly lower than that in previously reported studies focusing on seawater, wetlands, and stormwater ($p < 0.05$) (Fig. 4 and Table S10). The inconsistency between f_{TMP} of coastal seawater in this study and literature in Fig. 4 is possibly due to the different terrestrial inputs (or sources) to these seawater DOM pools. Among the reported f_{TMP}, we observed high f_{TMP} from estuarine water samples drained through everglades (wetland) (McKay et al., 2017) while the coastal seawater samples collected in the current study were mostly from sandy shores (Fig. 1). Thus, it can be inferred that DOM generated in highly productive wetlands can be efficient in ^{3}DOM* production, which is consistent with the high f_{TMP} in the observation (Fig. 4). It should be noted that DOM in estuarine water and nearshore seawater, may contain different proportions of terrestrial input from disparate land covers, which may exhibit different f_{TMP}. Thus, further study is recommended to investigate f_{TMP} of estuarine and nearshore samples drained from disparate land covers. Furthermore, f_{TMP} of offshore seawater (open ocean) is much less reported where pollutants were also detected (Biel-Maeso et al., 2018).

Furthermore, the average f_{TMP} of our freshwater samples (i.e., reservoirs) was similar to that of rivers, lakes, and wastewater (mostly effluent from treatment plants in the data) in the literature but the ranges were slightly wider for the literature data especially for lakes (Fig. 4). It is reasonable that DOM as well as the f_{TMP} show some similarities among reservoirs, rivers and lakes because reservoirs show semi-lake/semi-river characteristics (He et al., 2020). The similarity between

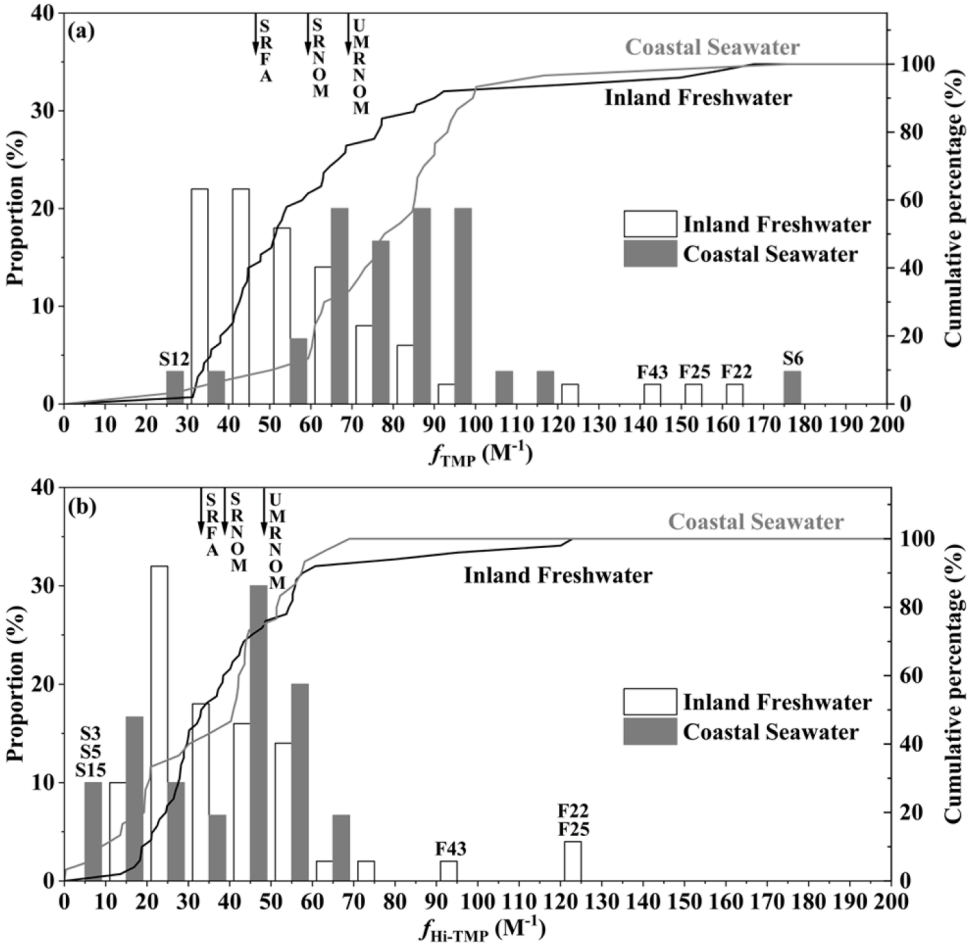

Fig. 3. Distribution of the quantum yield coefficients for photo-production of (a) ^{3}DOM* (f_{TMP}) and (b) Hi-^{3}DOM* ($f_{Hi\text{-}TMP}$) in inland freshwater (n = 50) and coastal seawater (n = 30) samples. The proportions were calculated within a bin size of 10 M^{-1}. SRFA: Suwannee River Fulvic Acid; SRNOM: Suwannee River Natural Organic Matter; UMRNOM: Upper Mississippi River Natural Organic Matter. For the sample codes, refer Tables S6 and S7.

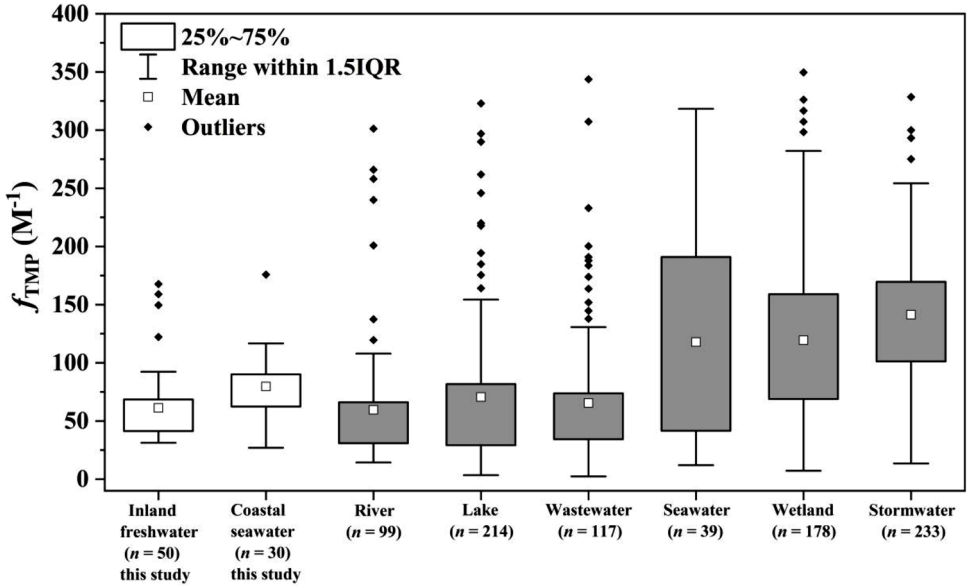

Fig. 4. Comparison of quantum yield coefficients (f_{TMP}) in the inland freshwater and coastal seawater samples determined in this study and those in literature for other types of water bodies (IQR: interquartile range, and data in Table S18).

f_{TMP} of reservoir and wastewater effluent is not well understood because they are generally from different sources (terrestrial and microbial sources for reservoirs and wastewater (Guo et al., 2023b; Zhou et al., 2019)), which generally behave differently in quantum yield (Ossola et al., 2021).

However, it is known that treatment methods such as UV irradiation, chlorination, and ozonation, affect f_{TMP} of wastewater (Wan et al., 2022). Thus, it is worth characterizing DOM from these natural waters and wastewater effluents to understand their similarity in f_{TMP}. Furthermore, the wider ranges for freshwater data in the literature were likely due to the higher diversity of samples from regions in the world (e.g., 214 lake samples collected from North America, North, Central and South Europe, Central East Asia, and Antarctic). Our experimental results additionally supplemented the unknown f_{TMP} of DOM in inland freshwater and coastal seawater in the northwestern Pacific region (Fig. 1). Nevertheless, additional investigation is still needed for quantum yield data (not only f_{TMP}) especially in tropical areas (South America, Africa, and East Asia) as pointed by Ossola et al. (2021).

3.3. Quantum yield coefficient of Hi-^{3}DOM* ($f_{Hi\text{-}TMP}$)

$f_{Hi\text{-}TMP}$ of the freshwater samples ranged from 13.5 M^{-1} at the Arakawa dam (F50) to 123 M^{-1} at the Shimokubo dam (F22), while $f_{Hi\text{-}TMP}$ of the coastal seawater samples was observed to be as low as 0.37 M^{-1} in Sagami Bay (S5) and the highest $f_{Hi\text{-}TMP}$ was 69.0 M^{-1} at coastal seawater near Hachinohe city (S8) (Fig. 3b and Table S9). The average $f_{Hi\text{-}TMP}$ of freshwater samples was 40.7 M^{-1}, which was not significantly higher than the average $f_{Hi\text{-}TMP}$ (36.0 M^{-1}) in coastal seawater samples ($p = 0.31$). The corresponding proportions of Hi-^{3}DOM* to ^{3}DOM* (denoted as %Hi-^{3}DOM*) ranged from 34.2 % at the Ikeda dam (F39) to 76.3 % at the Yagisawa dam (F21) for freshwater and from 0.41 % at Sagami Bay (S5) to 74.8 % at the western part of Ise bay (S26) for coastal seawater samples. The overall averaged%Hi-^{3}DOM* of 65.4 % in the freshwater samples was significantly higher than that in coastal seawater with an average of 45.4 %.

The%Hi-^{3}DOM* in the coastal seawater samples ranged wider (nearly 0 %–74.8 %) compared to the freshwater samples (34.3 %–76.3 %), indicating a high variability in the reactivity of ^{3}DOM* in coastal seawater. This could be attributed to the various sources (e.g., riverine input and algal production) of coastal seawater DOM that contribute to the varying amounts of Hi-^{3}DOM* precursors. In addition, coastal seawater components, such as antioxidants (phenolic moieties) and the abundant halide ions possibly quench Hi-^{3}DOM*. Given that the concentration of phenolic antioxidants was one order of magnitude lower in seawater DOM than that in freshwater DOM (terrestrially derived) (Guo et al., 2021), quenching of Hi-^{3}DOM* by phenolic antioxidants may not be predominant in seawater. Furthermore, given the negative correlation between salinity/conductivity and%Hi-^{3}DOM* (Fig. 5), quenching of Hi-^{3}DOM* by the abundant halide ions was highly probable, which could explain the lower average of%Hi-^{3}DOM*in coastal seawater than in freshwater samples.

The average%Hi-^{3}DOM* for freshwater samples (65.4 %) was comparable to that of wastewater effluent organic matter (65 %) (Zhou et al., 2019) despite their difference in the major sources (terrestrial freshwater samples vs microbial wastewater effluent organic matter). A previous study reported that microbial derived DOM showed a higher%

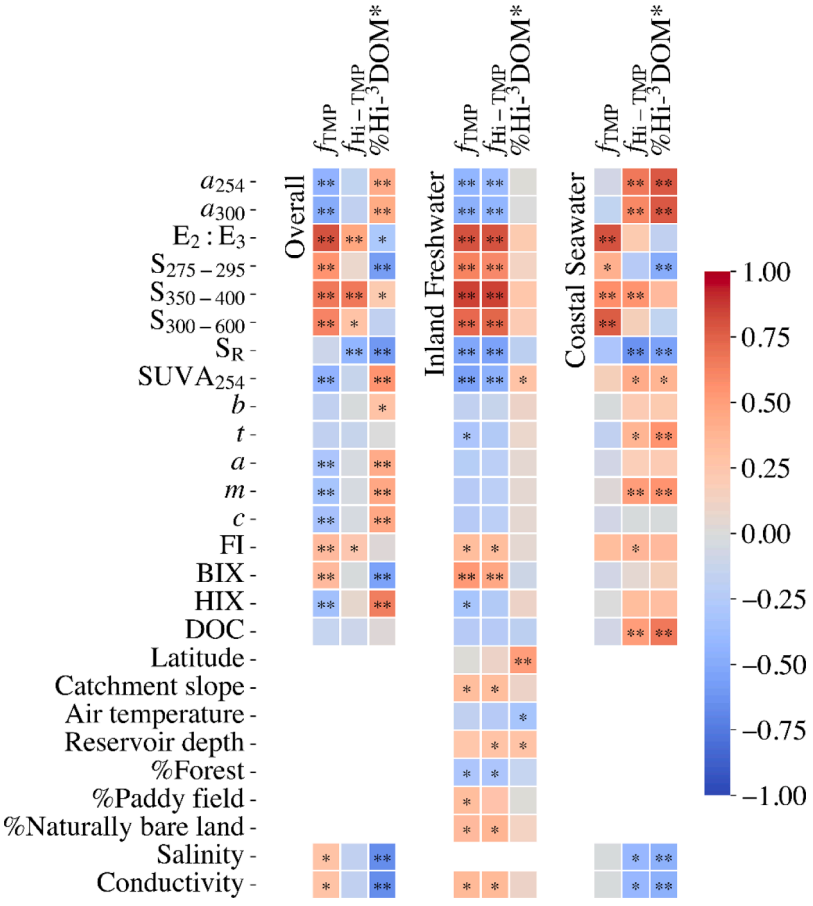

Fig. 5. Correlation matrix between the quantum yield coefficients (f_{TMP}, $f_{Hi\text{-}TMP}$, and %Hi-^{3}DOM*) and bulk water property (including catchment and reservoir characteristics) in the overall dataset, inland freshwater, and coastal seawater samples (*: $p < 0.05$, **: $p < 0.01$). %Forest is the areal proportion of forests in a catchment, including evergreen/deciduous coniferous/broadleaf forests (natural and secondary forests and planation). Some insignificant correlations were not shown here and were detailed in Figure S2).

Hi-^{3}DOM* than terrestrially derived DOM (Zhou et al., 2019). Thus, other factors such as degrees of photobleaching and humification may determine%Hi-^{3}DOM* because these processes influence the contents of ^{3}DOM* precursors and quenchers (Helms et al., 2014). Since the precursors of Hi-^{3}DOM* were suggested to be aromatic ketones (Zhou et al., 2017; Zhou et al., 2019), humification of freshwater DOM likely contributes more aryl ketones acting as Hi-^{3}DOM* precursors (Cao and Schmidt-Rohr, 2018). These results serve as the first dataset ever showing comparable ranges of %Hi-^{3}DOM* of freshwater and coastal seawater, which provides insights into the reactivity of ^{3}DOM* in the aquatic environment.

3.4. Correlation between quantum yield coefficients and bulk water properties

3.4.1. f_{TMP} and water properties in the overall dataset

In the overall dataset, significant correlations were observed between f_{TMP} and various bulk water properties, including a_{254}, a_{300}, E_2:E_3, $S_{275-295}$, $S_{350-400}$, $S_{300-600}$, SUVA$_{254}$, *a, m, c*, FI, BIX, HIX, and salinity/conductivity. Among them, strong correlations were observed between f_{TMP} and E_2:E_3, $S_{350-400}$, and $S_{300-600}$ (r = 0.80,0.66, and 0.61, respectively) (Fig. 5 and Table S11). E_2:E_3 showed the strongest correlation with f_{TMP} (r = 0.80), whereas previous studies have often observed stronger correlations of f_{TMP} with spectral slopes than E_2:E_3 (Ossola et al., 2021; Peterson et al., 2012; Wasswa et al., 2020). Thus, these correlations suggest that rather than spectral slopes, E_2:E_3 could be a predicator suitable for modeling diverse water properties covering inland freshwater and coastal seawater. This could be because spectral slopes take all spectral information for a specific range (i.e., 275 to 295 nm, 350 to 400 nm, and 300 to 600 nm) (Text S3), which could be different among particular sample types. On the contrary, E_2:E_3 only uses the absorbance at 254 nm and 365 nm of the DOM absorption spectra, which is not as specific as spectral slopes and thus describe a key optical property in a comparable manner. Moreover, this may also stem from the important roles that are closely related to aromatic structure of DOM as it can be characterized by light absorption at 254 nm (SUVA$_{254}$) (Weishaar et al., 2003). Thus, the E_2:E_3 seems a better predicator for modeling quantum yield of diverse water types than spectral slopes.

3.4.2. f_{TMP} and water properties in freshwater samples

In freshwater samples, f_{TMP} was significantly correlated with multiple bulk water properties, including a_{254}, a_{300}, E_2:E_3, $S_{275-295}$, $S_{350-400}$, $S_{300-600}$, S_R, SUVA$_{254}$, *t*, FI, BIX, HIX, and conductivity (Figs. 5 and Table S12). Strong correlations were observed between f_{TMP} and E_2:E_3, $S_{350-400}$, $S_{300-600}$, and $S_{275-295}$ (r = 0.81, 0.85, 0.72, and 0.63, respectively), which were similar to those in the overall dataset, whereas f_{TMP} showed the strongest correlation with $S_{350-400}$ (r = 0.85). A strong correlation was previously observed between $S_{350-400}$ and Φ_{1O2} (r = 0.84) in the same freshwater samples (Guo et al., 2023b). $S_{350-400}$ represents the relatively refractory DOM that is resistant to photodegradation, while $S_{275-295}$ reflects photolabile components (Grunert et al., 2018; Helms et al., 2013). Thus, the refractory components of DOM seem influential in both the ^{3}DOM* and $^1O_2$ production in inland freshwater. f_{TMP} was strongly correlated with the quantum yield for photo-production of $^1O_2$ (Φ_{1O2}), determined in the same freshwater samples previously (Guo et al., 2023b) (r^2 = 0.87, Figure S3). This is consistent with the known mechanism by which $^1O_2$ is produced via the energy transfer between ^{3}DOM* and O_2 (McNeill and Canonica, 2016). Considering the known reaction mechanism between ^{3}DOM* and TMP (electron-transfer) (Rosario-Ortiz and Canonica, 2016), the strong correlation indicates that the DOM molecules that can photochemically (via triplet-states) induce electron-transfer reaction can also induce energy-transfer to oxygen molecules in the freshwater samples. Interestingly, the correlation with conductivity was stronger (r = 0.36) than that observed for the overall dataset (r = 0.28). This indicates that inorganic ions in the freshwater samples can accelerate the production of ^{3}DOM*. This is possibly due to the decrease of decay rate constant of ^{3}DOM* along with an increase in ionic strength, which inhibits the ^{3}DOM*-induced electron transfer reactions within the DOM aggerates (Parker et al., 2013).

The f_{TMP} also significantly correlated with many catchment characteristics of the freshwater, including land cover ratio of forests (%Forest), paddy field, and naturally bare land, and catchment slope (Figs. 5 and S3). f_{TMP} showed a negative correlation (r = −0.30) with forest cover (areal ratio: 45 %–97 %) in freshwater catchments (%Forest in Fig. 5), and the forest proportion was positively correlated to DOC concentration (Figure S4). Thus, forest coverage possibly determines DOM in reservoir catchments, which is characterized by a relatively low f_{TMP}. In contrast, the proportions of paddy fields (0 %–20 %) and bare land (0 %–5 %) were positively correlated with f_{TMP} (r = 0.31 and 0.52, Figure S4). The proportion of paddy fields correlated positively with molecular indicators (E_2:E_3, $S_{350-400}$, and $S_{300-600}$), inferring that more DOM input from paddy field cover contributes to more low-molecular-weight components (Peuravuori and Pihlaja, 1997). Meanwhile, the proportion of naturally bare land positively correlated with BIX and negatively correlated with HIX, indicating that DOM is likely microbial-derived (Figure S4). Hence, these results demonstrate that bare land and paddy fields contribute DOM with relatively low-molecular-weight components from microbial sources, which are efficient in ^{3}DOM* production.

Furthermore, the positive correlation (r = 0.32) between the catchment slope (9.0°–34°) and f_{TMP} indicates that inland freshwater from a steeper catchment is more efficient in ^{3}DOM* generation. Additional analysis revealed a positive correlation between the catchment slope and E_2:E_3 and the three spectral slopes, as well as a negative correlation with HIX (Figure S4). These patterns indicate that a steeper catchment slope contributes DOM with fewer molecular sizes and fewer humified compounds to the reservoirs, possibly because of the shorter retention time of soil organic matter in the catchments. These relationships are consistent with previous studies reporting that DOM with more low-molecular-weight components is more efficient in producing ^{3}DOM* (Ossola et al., 2021).

3.4.3. f_{TMP} and water properties in coastal seawater samples

In contrast to freshwater samples, coastal seawater samples showed fewer correlations between f_{TMP} and bulk water properties than the overall dataset and freshwater samples (Fig. 5 and Table S13). The fewer correlations with optical properties (i.e., a_{254}, a_{300}, and SUVA$_{254}$, FI, BIX, and HIX) than that in freshwater can result from the relatively narrower ranges of optical properties for seawater samples. Only E_2:E_3, $S_{275-295}$, $S_{350-400}$, and $S_{300-600}$ showed significant correlations and correlations with E_2:E_3 and $S_{300-600}$ were strong with r of 0.80 and 0.77, respectively. Correlations with the optical properties of a_{254}, a_{300}, and SUVA$_{254}$, FI, BIX, and HIX were not significant, in contrast to freshwater samples. Considering the relatively low SUVA$_{254}$ for coastal seawater (Table S7), these results suggested that non-aromatic components possibly account for a major portion of coastal seawater DOM, among which carbonyl and olefinic structures are possibly responsible for ^{3}DOM* production, as previously reported (Seidel et al., 2022). Alternatively, this may suggest that the aromatic structures in coastal seawater DOM are efficient in utilizing light to produce ^{3}DOM*. These findings indicate that the major DOM components responsible for ^{3}DOM* production differ between inland freshwater and coastal seawater, possibly in terms of their molecular size and aromaticity. It is also possible that forest-derived aromatic components mask and further quench the photo-reactivity of non-aromatic components, resulting in a lower f_{TMP}. Since the contents of these structures acting as quenchers have been reported to be higher in terrestrial freshwater DOM than seawater DOM (Guo et al., 2021), such a quenching effect is highly probable. Thus, our next challenge is the investigation of specific organic components/structures controlling f_{TMP} to better understand the photo-reactivity of environmental water, while the actual reactivity of

^{3}DOM* in the water environment needs to be investigated in parallel with the determination of TMP.

Among the spectral slopes, f_{TMP} exhibited the strongest correlation with $S_{300-600}$ ($r = 0.77$), whereas in the freshwater samples, the strongest correlation was shown with $S_{350-400}$ ($r = 0.85$). The correlation coefficient between f_{TMP} and each spectral slope (e.g., $S_{275-295}$) for inland freshwater was different from the corresponding coefficient for coastal seawater (Fig. 6a) while the correlation coefficient between f_{TMP} and E_2:E_3 in coastal seawater was similar to that in inland freshwater ($r = 0.80$) (Fig. 6b). This further indicates that E_2:E_3 could be a more practical predictor than spectral slopes for modeling f_{TMP} in a diverse sample set containing freshwater and seawater.

3.4.4. $f_{Hi\text{-}TMP}$ and water properties

$f_{Hi\text{-}TMP}$ was significantly correlated with E_2:E_3, $S_{350-400}$, $S_{300-600}$, S_R, and FI, among which only $S_{350-400}$ was strongly correlated with $f_{Hi\text{-}TMP}$ ($r = 0.66$), in the overall dataset (Fig. 5). In freshwater samples, similar significant correlations were observed between bulk water properties and $f_{Hi\text{-}TMP}$ as those observed for f_{TMP}, which was reasonable considering the relatively high%Hi-^{3}DOM* in freshwater DOM (> 34.2 %, Table S9). The correlation between $f_{Hi\text{-}TMP}$ and the area of naturally bare land ($r = 0.53$) was slightly stronger than that of f_{TMP}, indicating DOM originated from naturally bare land is abundant in Hi-^{3}DOM* precursors. The conductivity was positively correlated to both $f_{Hi\text{-}TMP}$ and f_{TMP} ($r = 0.35$ and 0.36, respectively), suggesting high conductivity is beneficial for both production of both ^{3}DOM* and Hi-^{3}DOM* in freshwater samples. This can be due to that an increase in ionic strength that can decrease the decay rate constant of ^{3}DOM* (Parker et al., 2013).

In the coastal seawater samples, more significant correlations were observed between $f_{Hi\text{-}TMP}$ than f_{TMP} and bulk water properties (Table S13). These water properties included a_{254}, a_{300}, $S_{350-400}$, S_R, $SUVA_{254}$, t, m, FI, DOC and salinity/conductivity. Notably, most of the correlation coefficients between $f_{Hi\text{-}TMP}$ and bulk water properties were the inverse to those for freshwater samples. For instance, the correlations with a_{254}, a_{300}, $SUVA_{254}$, t, and m were positive for coastal seawater but negative for inland freshwater (Fig. 5). This indicates different Hi-^{3}DOM* precursors in freshwater and coastal seawater DOM. Furthermore, the significant correlation between DOC concentration (range: 0.71 mgC/L–1.5 mgC/L) and $f_{Hi\text{-}TMP}$ was confirmed only for the seawater samples ($r = 0.51$, $p = 0.004$), for which DOC concentration also showed a positive correlation with%Hi-^{3}DOM* (Fig. 5). These results indicate that coastal seawater with higher DOC concentration can be more efficient in generating Hi-^{3}DOM* and thus Hi-^{3}DOM* precursors likely account for a major portion of coastal seawater DOM.

Salinity/conductivity was negatively correlated with $f_{Hi\text{-}TMP}$, possibly indicating the consumption of Hi-^{3}DOM* by salts in seawater, in contrast to the abovementioned possible promoting effect at low salinity levels in inland freshwater. The inhibitory effect in coastal seawater could be due to additional halide ions (Parker and Mitch, 2016), which preferentially consumed the more reactive Hi-^{3}DOM* (possibly microbial and algal origins) than low-energy ^{3}DOM* (Zhou et al., 2019). As ^{3}DOM* can react with halide ions to form halogen radicals (Parker and Mitch, 2016), we speculated that the reaction between Hi-^{3}DOM* and halide ions could play a more critical role in halogen radical generation in seawater than that of low-energy ^{3}DOM. Therefore, this reaction may be an important source of halogen radicals in sunlit seawater. Particularly, the Hi-^{3}DOM* may play an important role in producing Cl· (single Cl radical), as the energy requirement for oxidizing Cl^- to Cl· is high (2.5 V_{SHE}) (Zhang and Parker, 2018).

3.5. Empirical models of f_{TMP} and their application

In SLR modeling (Table S14), $S_{350-400}$ exhibited the best performance for estimating $f_{TMP\text{-}F\text{-}SLR}$ in freshwater samples ($r^2 = 0.72$, RMSE = 16.3, Eq. (4), Fig. 7). E_2:E_3 performed the best for estimating $f_{TMP\text{-}S\text{-}SLR}$ in coastal seawater samples ($r^2 = 0.63$ and RMSE = 15.5 (Eq. (5))) and for the overall dataset ($f_{TMP\text{-}SLR}$; $r^2 = 0.64$ and RMSE = 18.2 (Eq. (6))). It is worth noting that E_2:E_3 exhibited a strong estimation ability for all three datasets though the parameters of E_2:E_3-based SLR models differed (Table S14). Thus, E_2:E_3 may be a practical predictor for both freshwater and seawater. The current $f_{TMP\text{-}SLR}$ model is the only available tool for estimating f_{TMP} in seawater which is necessary for risk assessment of organic micropollutants in seawater. Further studies should be conducted to comprehensively clarify the applicability of the $f_{TMP\text{-}SLR}$ model in other types of water environments.

Inland freshwater :

$$f_{TMP-F-SLR} = 7705\ S_{350-400} - 65.41 \quad (4)$$

Coastal seawater :

$$f_{TMP-S-SLR} = 12.28E_2 : E_3 - 2.466 \quad (5)$$

Overall dataset :

$$f_{TMP-SLR} = 15.44\ E_2 : E_3 - 22.04 \quad (6)$$

Based on the OPLS analysis, E_2:E_3 and spectral slopes ($S_{275-295}$, $S_{300-600}$, and $S_{350-400}$) showed VIP scores greater than 1.0 (Tables S15−S16 and Figures S5−S7); thus, they were used for stepwise MLR modeling for each of the three datasets. The MLR model employed $S_{350-400}$ and BIX as predictors for freshwater samples ($f_{TMP\text{-}F\text{-}MLR}$, Eq. (7)), with an r^2 of 0.84 and RMSE of 12.3, and employed E_2:E_3 and $S_{300-600}$ for coastal seawater samples, with an r^2 of 0.66 and RMSE of 14.5 ($f_{TMP\text{-}S\text{-}MLR}$, Eq. (8)) (Fig. 7e and 7h). E_2:E_3 and $S_{350-400}$ were selected for modeling the overall dataset ($r^2 = 0.67$ and RMSE = 17.4, $f_{TMP-MLR}$, Eq. (9)).

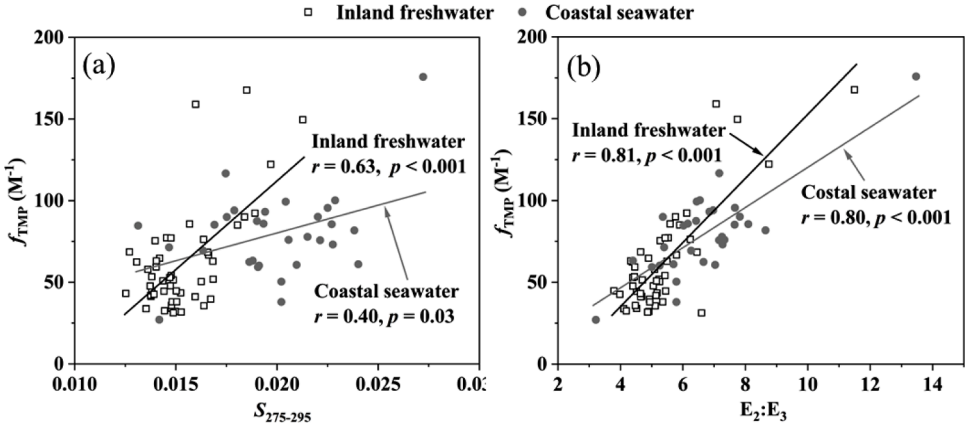

Fig. 6. Correlation plot between f_{TMP} and (a) $S_{275-295}$ and (b) E_2:E_3 of inland freshwater ($n = 50$) and coastal seawater ($n = 30$) samples.

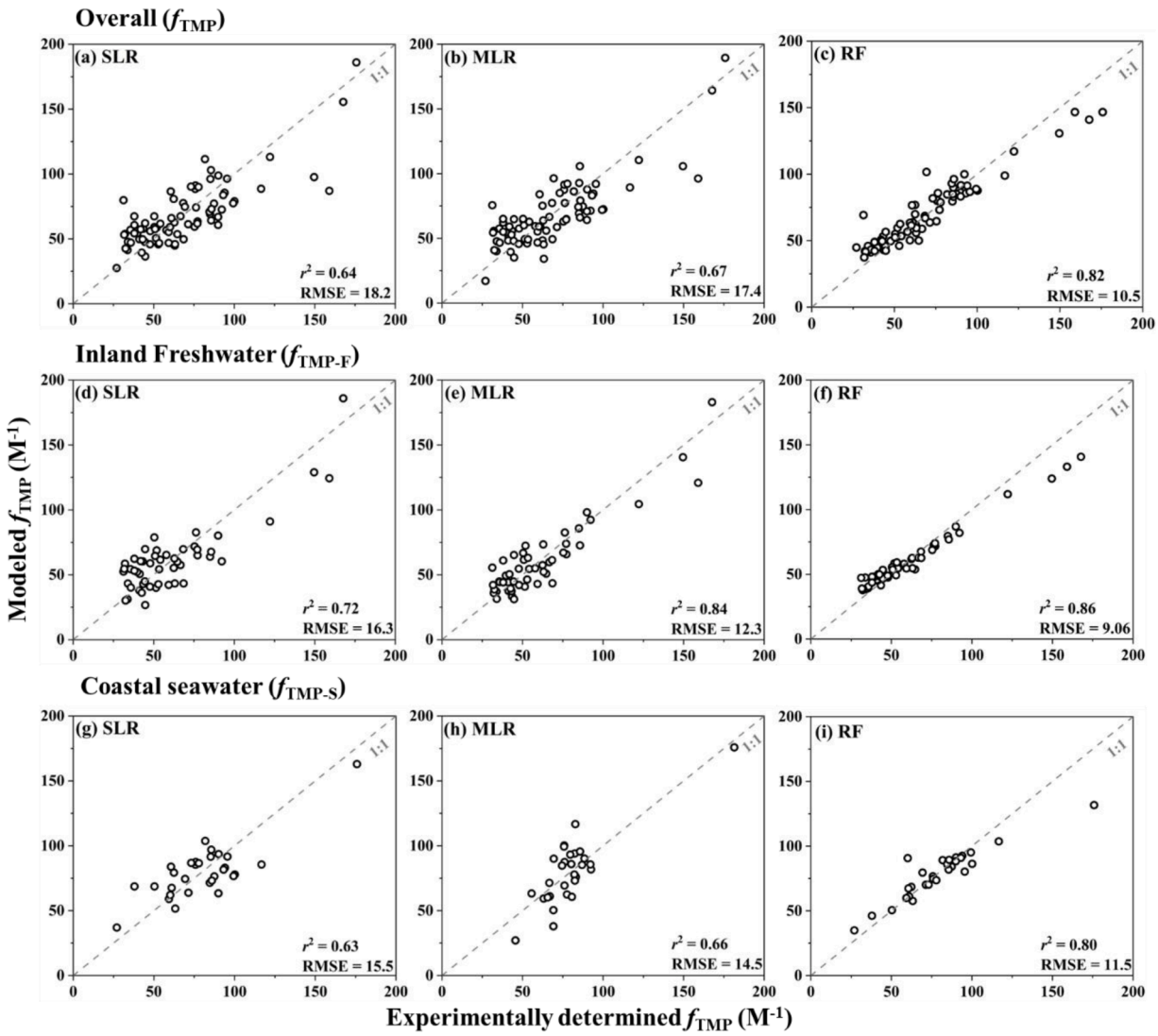

Fig. 7. Performance of the developed models in the (a-c) overall dataset (f_{TMP}), (d-f) inland freshwater samples ($f_{TMP\text{-}F}$), and (g-i) the coastal seawater samples ($f_{TMP\text{-}S}$).

$$\text{Inland freshwater}: \quad f_{TMP-F-MLR} = 6980\ S_{350-400} + 170.6\ \text{BIX} - 165.2 \tag{7}$$

$$\text{Coastal seawater}: \quad f_{TMP-S-MLR} = 428.2\ S_{300-600} + 8.017\ E_2 : E_3 + 16.79 \tag{8}$$

$$\text{Overall dataset}: \quad f_{TMP-MLR} = 1584\ S_{350-400} + 12.50\ E_2 : E_3 - 31.06 \tag{9}$$

Compared to the SLR models, $f_{TMP\text{-}F\text{-}MLR}$ (freshwater) exhibited a slightly increased performance, whereas $f_{TMP-MLR}$ (overall dataset) and $f_{TMP\text{-}S\text{-}MLR}$ (seawater) showed no substantial improvement. Expression of the MLR models depends on the data (i.e., water samples) because of the different bulk water properties between freshwater and coastal seawater samples (Fig. 2). Simultaneously, two of the MLR models suffered from multicolinearlity which usually occurred in previous MLR modeling (Du et al., 2018; McKay et al., 2017; Wasswa et al., 2020). The $S_{300-600}$ and E_2:E_3 in $f_{TMP\text{-}S\text{-}MLR}$ were significantly correlated ($r = 0.80$, $p < 0.01$) and the E_2:E_3 and another spectral slope, $S_{350-400}$ were correlated ($p < 0.01$, $r = 0.75$) in $f_{TMP-MLR}$. The $S_{350-400}$ and BIX in $f_{TMP\text{-}F\text{-}MLR}$ were not correlated ($r = 0.23$, $p = 0.11$). Thus, currently the SLR model based solely on E_2:E_3 (Eq. (6)) may be a practical model for estimating f_{TMP}.

RF models further decreased the RMSE from SLR and MLR, with r^2 = 0.86, 0.80, and 0.82, and RMSE = 9.06, 11.5, and 10.5, for freshwater, coastal seawater, and the overall dataset, respectively. The most important features (feature importance > 0.1, Table S17) were E_2:E_3, $S_{300-600}$ and $S_{350-400}$ for the overall dataset, $S_{350-400}$, E_2:E_3 and $S_{300-600}$ for the freshwater samples, and $S_{300-600}$, t, and FI for the coastal seawater samples. In all RF models, spectral slopes were selected as influential predictors, which generally exhibited a stronger correlation with quantum yield than E_2:E_3 (Ossola et al., 2021). However, overfitting has been observed for coastal seawater samples even after hyperparameter (Text S7). This is reasonable because a smaller dataset (i.e., coastal seawater samples vs freshwater samples) is more susceptible to overfitting (Kohavi and Sommerfield, 1995). Note that several water properties are needed in the estimation of f_{TMP} using the RF models (at least E_2:E_3, $S_{350-400}$, $S_{300-600}$, t, and FI), which makes it more time-consuming than the application of the SLR models.

The applications of linear regression and RF models to the samples of lakes (L3, L7, and L8), ponds (L1, L2, and L4−L6), and reference NOM (SRFA, SRNOM, and Upper Mississippi River natural organic matter (UMRNOM)) resulted in an RMSE of approximately 40 M^{-1} (38.5 to 46.0 M^{-1}), except for $f_{TMP\text{-}F\text{-}SLR}$ (Eq. (4)) showing the highest RMSE of 60.0 M^{-1} (Table S18). Interestingly, regarding SLR models, the functions of E_2:E_3 performed better for the lake, pond, and reference NOM samples

than the function of $S_{350-400}$ ($f_{TMP\text{-}F\text{-}SLR}$, Eq. (4)) (Table S18). This result also supports the significance of E_2:E_3 as a practical predicator for estimating f_{TMP} in a diverse sample set while $S_{350-400}$ seems to be valid only for the reservoir samples. The MLR models slightly outperformed SLR models for the coastal seawater samples and the overall dataset. When estimating f_{TMP} for lake/pond and reference NOM, the RF models did not obviously outperform SLR and MLR models, although RF showed better performance than the other models for freshwater and coastal seawater samples. Therefore, we concluded that the SLR model (i.e., the linear function of E_2:E_3, $f_{TMP\text{-}SLR}$, Eq. (6)) could be a practical model for the wide estimation of f_{TMP}, whereas the RF models are more accurate than the SLR models for the modelled samples.

4. Conclusions

This study comparably quantified quantum yield coefficient for photo-production of both ^{3}DOM* and Hi-^{3}DOM* in coastal seawater and inland freshwater and developed available f_{TMP} estimation models that can be applied to both freshwater and seawater. Coastal seawater DOM was found to be mainly dominated by microbial DOM, which contained more low-molecular-weight components and was lower in light absorption compared with freshwater (reservoir) DOM which was mainly from terrestrial sources. f_{TMP} in average was higher in coastal seawater (79.7 M^{-1}) than in freshwater samples (61.2 M^{-1}). For the first time, we observed the proportion of Hi-^{3}DOM* varied greatly in coastal seawater (0.4 % to 71.8 %) compared to the range of 34.3 % to 76.3 % in freshwater samples.

Catchment characteristics of inland freshwater such as different land covers and catchment slopes can affect f_{TMP}. E_2:E_3 and spectral slopes were both significantly correlated with f_{TMP} in coastal seawater and freshwater samples, which were used for further modeling f_{TMP}. The model analyses revealed that E_2:E_3 was possibly a more reliable parameter in SLR modeling than spectral slopes for a wide estimation of f_{TMP} including both freshwater and seawater, even though spectral slopes usually outperform than E_2:E_3. Machine-learning based RF showed the best performance in estimating f_{TMP} regardless of sample types, while a larger dataset is recommended for a better model. Since ^{3}DOM* plays important roles in the natural degradation processes of organic pollutants and global carbon cycle in both inland freshwater and seawater, the modeling of f_{TMP} and the investigation of highly reactive ^{3}DOM* are of practical significance in environmental management.

CRediT authorship contribution statement

Zhongyu Guo: Conceptualization, Formal analysis, Funding acquisition, Investigation, Methodology, Visualization, Writing – original draft. **Tingting Wang:** Formal analysis, Methodology, Visualization, Writing – review & editing. **Hidetaka Ichiyanagi:** Formal analysis, Funding acquisition, Methodology, Project administration, Resources, Writing – review & editing. **Mohamed Ateia:** Writing – review & editing, Formal analysis. **Guo Chen:** Investigation, Writing – review & editing. **Jieqiong Wang:** Formal analysis, Investigation, Writing – review & editing. **Manabu Fujii:** Supervision, Writing – review & editing. **Kaichii En:** Formal analysis, Methodology. **Tiansheng Li:** Investigation, Methodology. **Rumi Sohrin:** Resources. **Chihiro Yoshimura:** Funding acquisition, Supervision, Project administration, Resources, Writing – review & editing.

Declaration of competing interest

The authors declare that they have no known competing financial interests or personal relationships that could have appeared to influence the work reported in this paper.

Data availability

Data will be made available on request.

Acknowledgement

This research was supported by Water Resources Environment Center (Grant number 2021-03) the Japan Society for the Promotion of Science (JSPS KAKENHI, 21H01462 and 22J12590) and JST SPRING (JPMJSP2125). The authors appreciate Li Cui and Kirana Nadhila for their support in the experimental work, Dilini Kodikara for the kind help in language proof and Dr. Toru Suzuki for collecting and analyzing the land cover of reservoir catchments. We also appreciate Jiefeng Li, Ye Zhang, Zhaohua Fang, Zhengjun Qian, and members of the SURUME project for their effort in sampling and delivering the seawater samples.

Supplementary materials

Supplementary material associated with this article can be found, in the online version, at doi:10.1016/j.watres.2024.121260.

References

Aluwihare, L.I., Repeta, D.J., Chen, R.F., 1997. A major biopolymeric component to dissolved organic carbon in surface sea water. Nature 387, 166–169. https://doi.org/10.1038/387166a0.

Benner, R., Pakulski, J.D., McCarthy, M., Hedges, J.I., Hatcher, P.G., 1992. Bulk chemical characteristics of dissolved organic matter in the ocean. Science 255, 1561–1564. https://doi.org/10.1126/science.255.5051.1561.

Berg, S.M., Wammer, K.H., Remucal, C.K., 2023. Dissolved organic matter photoreactivity is determined by its optical properties, redox activity, and molecular composition. Environ. Sci. Technol. 57, 6703–6711. https://doi.org/10.1021/acs.est.3c01157.

Biel-Maeso, M., Baena-Nogueras, R.M., Corada-Fernández, C., Lara-Martín, P.A., 2018. Occurrence, distribution and environmental risk of pharmaceutically active compounds (PhACs) in coastal and ocean waters from the Gulf of Cadiz (SW Spain). Sci. Total Environ. 612, 649–659. https://doi.org/10.1016/j.scitotenv.2017.08.279.

Boreen, A.L., Arnold, W.A., McNeill, K., 2003. Photodegradation of pharmaceuticals in the aquatic environment: a review. Aquat. Sci. 65, 320–341. https://doi.org/10.1007/s00027-003-0672-7.

Cao, X., Schmidt-Rohr, K., 2018. Abundant nonprotonated aromatic and oxygen-bonded carbons make humic substances distinct from biopolymers. Environ. Sci. Technol. Lett. 5, 476–480. https://doi.org/10.1021/acs.estlett.8b00107.

Carena, L., García-Gil, Á., Marugán, J., Vione, D., 2023. Global modeling of lake-water indirect photochemistry based on the equivalent monochromatic wavelength approximation: the case of the triplet states of chromophoric dissolved organic matter. Water Res. 241, 120153 https://doi.org/10.1016/j.watres.2023.120153.

Chen, X., Wang, J.Q., Chen, J.W., Zhou, C.Z., Cui, F.F., Sun, G.X., 2019. Photodegradation of 2-(2-hydroxy-5-methylphenyl)benzotriazole (UV-P) in coastal seawaters: important role of DOM. J. Environ. Sci. 85, 129–137. https://doi.org/10.1016/j.jes.2019.05.017.

Chen, Y., Hozalski, R.M., Olmanson, L.G., Page, B.P., Finlay, J.C., Brezonik, P.L., Arnold, W.A., 2020. Prediction of photochemically produced reactive intermediates in surface waters via satellite remote sensing. Environ. Sci. Technol. 54, 6671–6681. https://doi.org/10.1021/acs.est.0c00344.

Coble, P.G., 1996. Characterization of marine and terrestrial DOM in seawater using excitation-emission matrix spectroscopy. Mar. Chem. 51, 325–346. https://doi.org/10.1016/0304-4203(95)00062-3.

D'Andrilli, J., Silverman, V., Buckley, S., Rosario-Ortiz, F.L., 2022. Inferring ecosystem function from dissolved organic matter optical properties: a critical review. Environ. Sci. Technol. 56, 11146–11161. https://doi.org/10.1021/acs.est.2c04240.

De Laurentiis, E., Buoso, S., Maurino, V., Minero, C., Vione, D., 2013. Optical and photochemical characterization of chromophoric dissolved organic matter from Lakes in Terra Nova Bay, Antarctica. Evidence of considerable photoreactivity in an extreme environment. Environ. Sci. Technol. 47, 14089–14098. https://doi.org/10.1021/es403364z.

Dittmar, T., Stubbins, A., 2014. Dissolved organic matter in aquatic systems. Treatise on Geochemistry. Elsevier, pp. 125–156. https://doi.org/10.1016/B978-0-08-095975-7.01010-X.

Du, Z., He, Y., Fan, J., Fu, H., Zheng, S., Xu, Z., Qu, X., Kong, A., Zhu, D., 2018. Predicting apparent singlet oxygen quantum yields of dissolved black carbon and humic substances using spectroscopic indices. Chemosphere 194, 405–413. https://doi.org/10.1016/j.chemosphere.2017.11.172.

Erickson, P.R., Moor, K.J., Werner, J.J., Latch, D.E., Arnold, W.A., McNeill, K., 2018. Singlet oxygen phosphorescence as a probe for triplet-state dissolved organic matter reactivity. Environ. Sci. Technol. 52, 9170–9178. https://doi.org/10.1021/acs.est.8b02379.

Glover, C.M., Rosario-Ortiz, F.L., 2013. Impact of halides on the photoproduction of reactive intermediates from organic matter. Environ. Sci. Technol. 47, 13949–13956. https://doi.org/10.1021/es4026886.
Grunert, B.K., Mouw, C.B., Ciochetto, A.B., 2018. Characterizing CDOM spectral variability across diverse regions and spectral ranges: characterizing CDOM spectral variability. Glob. Biogeochem. Cycles 32, 57–77. https://doi.org/10.1002/2017GB005756.
Guo, Z.Y., Kodikara, D., Albi, L.S., Hatano, Y., Chen, G., Yoshimura, C., Wang, J.Q., 2023a. Photodegradation of organic micropollutants in aquatic environment: importance, factors and processes. Water Res. 231, 118236 https://doi.org/10.1016/j.watres.2022.118236.
Guo, Z.Y., Wang, J.Q., Chen, X., Cui, F.F., Wang, T.T., Zhou, C.Z., Song, G.B., Zhang, S.Y., Chen, J.W., 2021. Photochemistry of dissolved organic matter extracted from coastal seawater: excited triplet-states and contents of phenolic moieties. Water Res. 188, 116568 https://doi.org/10.1016/j.watres.2020.116568.
Guo, Z.Y., Wang, T.T., Chen, G., Wang, J.Q., Fujii, M., Yoshimura, C., 2023b. Apparent quantum yield for photo-production of singlet oxygen in reservoirs and its relation to the water matrix. Water Res. 120456 https://doi.org/10.1016/j.watres.2023.120456.
He, D., Wang, K., Pang, Y., He, C., Li, P., Li, Y., Xiao, S., Shi, Q., Sun, Y., 2020. Hydrological management constraints on the chemistry of dissolved organic matter in the Three Gorges Reservoir. Water Res. 187, 116413 https://doi.org/10.1016/j.watres.2020.116413.
Helms, J.R., Mao, J., Stubbins, A., Schmidt-Rohr, K., Spencer, R.G.M., Hernes, P.J., Mopper, K., 2014. Loss of optical and molecular indicators of terrigenous dissolved organic matter during long-term photobleaching. Aquat. Sci. 76, 353–373. https://doi.org/10.1007/s00027-014-0340-0.
Helms, J.R., Stubbins, A., Perdue, E.M., Green, N.W., Chen, H., Mopper, K., 2013. Photochemical bleaching of oceanic dissolved organic matter and its effect on absorption spectral slope and fluorescence. Mar. Chem. 155, 81–91. https://doi.org/10.1016/j.marchem.2013.05.015.
Helms, J.R., Stubbins, A., Ritchie, J.D., Minor, E.C., Kieber, D.J., Mopper, K., 2008. Absorption spectral slopes and slope ratios as indicators of molecular weight, source, and photobleaching of chromophoric dissolved organic matter. Limnol. Oceanogr. 53, 955–969. https://doi.org/10.4319/lo.2008.53.3.0955.
Huguet, A., Vacher, L., Relexans, S., Saubusse, S., Froidefond, J.M., Parlanti, E., 2009. Properties of fluorescent dissolved organic matter in the gironde estuary. Org. Geochem. 40, 706–719. https://doi.org/10.1016/j.orggeochem.2009.03.002.
Kieber, D.J., McDaniel, J., Mopper, K., 1989. Photochemical source of biological substrates in sea water: implications for carbon cycling. Nature 341, 637–639. https://doi.org/10.1038/341637a0.
Kohavi, R., Sommerfield, D., 1995. Feature subset selection using the wrapper method: overfitting and dynamic search space topology. In: Proceedings of the First International Conference on Knowledge Discovery and Data Mining. KDD, pp. 192–197.
Laszakovits, J.R., Berg, S.M., Anderson, B.G., O'Brien, J.E., Wammer, K.H., Sharpless, C. M., 2017. P-Nitroanisole/pyridine and p-Nitroacetophenone/pyridine actinometers revisited: quantum yield in comparison to ferrioxalate. Environ. Sci. Technol. Lett. 4, 11–14. https://doi.org/10.1021/acs.estlett.6b00422.
Lian, L., Yan, S., Zhou, H., Song, W., 2020. Overview of the phototransformation of wastewater effluents by high-resolution mass spectrometry. Environ. Sci. Technol. 54, 1816–1826. https://doi.org/10.1021/acs.est.9b04669.
Liao, Z., Lu, J., Xie, K., Wang, Y., Yuan, Y., 2023. Prediction of photochemical properties of dissolved organic matter using machine learning. Environ. Sci. Technol. https://doi.org/10.1021/acs.est.2c07545 acs.est.2c07545.
Lindner, T., Puck, J., Verbeke, A., 2022. Beyond addressing multicollinearity: robust quantitative analysis and machine learning in international business research. J. Int. Bus. Stud. 53, 1307–1314. https://doi.org/10.1057/s41267-022-00549-z.
McCabe, A.J., Arnold, W.A., 2018. Multiple linear regression models to predict the formation efficiency of triplet excited states of dissolved organic matter in temperate wetlands. Limnol. Oceanogr. 63, 1992–2014. https://doi.org/10.1002/lno.10820.
McCabe, A.J., Arnold, W.A., 2017. Reactivity of triplet excited states of dissolved natural organic matter in stormflow from mixed-use watersheds. Environ. Sci. Technol. 51, 9718–9728. https://doi.org/10.1021/acs.est.7b01914.
McCabe, A.J., Arnold, W.A., 2016. Seasonal and spatial variabilities in the water chemistry of prairie pothole wetlands influence the photoproduction of reactive intermediates. Chemosphere 155, 640–647. https://doi.org/10.1016/j.chemosphere.2016.04.078.
McKay, G., Huang, W., Romera-Castillo, C., Crouch, J.E., Rosario-Ortiz, F.L., Jaffé, R., 2017. Predicting reactive intermediate quantum yields from dissolved organic matter photolysis using optical properties and antioxidant capacity. Environ. Sci. Technol. 51, 5404–5413. https://doi.org/10.1021/acs.est.6b06372.
McKnight, D.M., Boyer, E.W., Westerhoff, P.K., Doran, P.T., Kulbe, T., Andersen, D.T., 2001. Spectrofluorometric characterization of dissolved organic matter for indication of precursor organic material and aromaticity. Limnol. Oceanogr. 46, 38–48. https://doi.org/10.4319/lo.2001.46.1.0038.
McNeill, K., Canonica, S., 2016. Triplet state dissolved organic matter in aquatic photochemistry: reaction mechanisms, substrate scope, and photophysical properties. Environ. Sci. Process. Impacts 18, 1381–1399. https://doi.org/10.1039/c6em00408c.
Mopper, K., Kieber, D.J., 2000. Marine photochemistry and its impact on carbon cycling. The Effects of UV Radiation in the Marine Environment, pp. 101–129. https://doi.org/10.1017/CBO9780511535444.005, 10.
Ohno, T., 2002. Fluorescence inner-filtering correction for determining the humification index of dissolved organic matter. Environ. Sci. Technol. 36, 742–746. https://doi.org/10.1021/es0155276.
Osburn, C.L., Bianchi, T.S., 2016. Editorial: linking optical and chemical properties of dissolved organic matter in natural waters. Front. Mar. Sci. 3 https://doi.org/10.3389/fmars.2016.00223.
Osburn, C.L., Wigdahl, C.R., Fritz, S.C., Saros, J.E., 2011. Dissolved organic matter composition and photoreactivity in prairie lakes of the U.S. Great Plains. Limnol. Oceanogr. 56, 2371–2390. https://doi.org/10.4319/lo.2011.56.6.2371.
Ossola, R., Jönsson, O.M., Moor, K., McNeill, K., 2021. Singlet oxygen quantum yields in environmental waters. Chem. Rev. 121, 4100–4146. https://doi.org/10.1021/acs.chemrev.0c00781.
Parker, K.M., Mitch, W.A., 2016. Halogen radicals contribute to photooxidation in coastal and estuarine waters. Proc. Natl. Acad. Sci. U.S.A. 113, 5868–5873. https://doi.org/10.1073/pnas.1602595113.
Parker, K.M., Pignatello, J.J., Mitch, W.A., 2013. Influence of ionic strength on triplet-state natural organic matter loss by energy transfer and electron transfer pathways. Environ. Sci. Technol. 47, 10987–10994. https://doi.org/10.1021/es401900j.
Peterson, B.M., McNally, A.M., Cory, R.M., Thoemke, J.D., Cotner, J.B., McNeill, K., 2012. Spatial and temporal distribution of singlet oxygen in Lake Superior. Environ. Sci. Technol. 46, 7222–7229. https://doi.org/10.1021/es301105e.
Peuravuori, J., Pihlaja, K., 1997. Molecular size distribution and spectroscopic properties of aquatic humic substances. Anal. Chim. Acta 337, 133–149. https://doi.org/10.1016/S0003-2670(96)00412-6.
Rosario-Ortiz, F.L., Canonica, S., 2016. Probe compounds to assess the photochemical activity of dissolved organic matter. Environ. Sci. Technol. 50, 12532–12547. https://doi.org/10.1021/acs.est.6b02776.
Seidel, M., Vemulapalli, S.P.B., Mathieu, D., Dittmar, T., 2022. Marine dissolved organic matter shares thousands of molecular formulae yet differs structurally across major water masses. Environ. Sci. Technol. 56, 3758–3769. https://doi.org/10.1021/acs.est.1c04566.
Spencer, R.G.M., Butler, K.D., Aiken, G.R., 2012. Dissolved organic carbon and chromophoric dissolved organic matter properties of rivers in the USA. J. Geophys. Res. 117 https://doi.org/10.1029/2011JG001928.
Thévenot, E.A., Roux, A., Xu, Y., Ezan, E., Junot, C., 2015. Analysis of the human adult urinary metabolome variations with age, body mass index, and gender by implementing a comprehensive workflow for univariate and OPLS statistical analyses. J. Proteome Res. 14, 3322–3335. https://doi.org/10.1021/acs.jproteome.5b00354.
Thornton, D.C.O., 2014. Dissolved organic matter (DOM) release by phytoplankton in the contemporary and future ocean. Eur. J. Phycol. 49, 20–46. https://doi.org/10.1080/09670262.2013.875596.
Vione, D., 2020. A critical view of the application of the APEX software (aqueous photochemistry of environmentally-occurring xenobiotics) to predict photoreaction kinetics in surface freshwaters. Molecules 25. https://doi.org/10.3390/molecules25010009.
Vione, D., Minella, M., Maurino, V., Minero, C., 2014. Indirect photochemistry in sunlit surface waters: photoinduced production of reactive transient species. Chem. Eur. J. 20, 10590–10606. https://doi.org/10.1002/chem.201400413.
Vione, D., Saglia, F., Pelazza, C., 2023. Possible effects of changes in carbonate concentration and river flow rate on photochemical reactions in temperate aquatic environments. Molecules 28, 7072. https://doi.org/10.3390/molecules28207072.
Wan, D., Wang, J., Chen, T., Xiang, W., Selvinsimpson, S., Chen, Y., 2022. Effect of disinfection on the photoreactivity of effluent organic matter and photodegradation of organic contaminants. Water Res. 219, 118552 https://doi.org/10.1016/j.watres.2022.118552.
Wang, H., Zhou, H.X., Ma, J.Z., Nie, J.X., Yan, S.W., Song, W.H., 2020. Triplet photochemistry of dissolved black carbon and its effects on the photochemical formation of reactive oxygen species. Environ. Sci. Technol. 54, 4903–4911. https://doi.org/10.1021/acs.est.0c00061.
Wang, J.Q., Chen, J.W., Qiao, X.L., Zhang, Y.N., Uddin, M., Guo, Z.Y., 2019. Disparate effects of DOM extracted from coastal seawaters and freshwaters on photodegradation of 2,4-Dihydroxybenzophenone. Water Res 151, 280–287. https://doi.org/10.1016/j.watres.2018.12.045.
Wang, Y., Fan, L., Jones, O.A.H., Roddick, F., 2021. Quantification of seasonal photo-induced formation of reactive intermediates in a municipal sewage lagoon upon sunlight exposure. Sci. Total Environ. 765, 142733 https://doi.org/10.1016/j.scitotenv.2020.142733.
Wasswa, J., Driscoll, C.T., Zeng, T., 2020. Photochemical characterization of surface waters from lakes in the Adirondack region of New York. Environ. Sci. Technol. 54, 10654–10667. https://doi.org/10.1021/acs.est.0c02811.
Weishaar, J.L., Aiken, G.R., Bergamaschi, B.A., Fram, M.S., Fujii, R., Mopper, K., 2003. Evaluation of specific ultraviolet absorbance as an indicator of the chemical composition and reactivity of dissolved organic carbon. Environ. Sci. Technol. 37, 4702–4708. https://doi.org/10.1021/es030360x.
Wenk, J., Canonica, S., 2012. Phenolic antioxidants inhibit the triplet-induced transformation of anilines and sulfonamide antibiotics in aqueous solution. Environ. Sci. Technol. 46, 5455–5462. https://doi.org/10.1021/es300485u.
Wenk, J., Nguyen, M.T., Nelson, K.L., 2019. Natural photosensitizers in constructed unit process wetlands: photochemical characterization and inactivation of pathogen indicator organisms. Environ. Sci. Technol. 53, 7724–7735. https://doi.org/10.1021/acs.est.9b01180.
Yan, S.W., Song, W.H., 2014. Photo-transformation of pharmaceutically active compounds in the aqueous environment: a review. Environ. Sci. Process. Impacts 16, 697–720. https://doi.org/10.1039/c3em00502j.
Zepp, R.G., Schlotzhauer, P.F., Sink, R.M., 1985. Photosensitized transformations involving electronic energy transfer in natural waters: role of humic substances. Environ. Sci. Technol. 19, 74–81. https://doi.org/10.1021/es00131a008.

Zhang, K., Parker, K.M., 2018. Halogen radical oxidants in natural and engineered aquatic systems. Environ. Sci. Technol. 52, 9579–9594. https://doi.org/10.1021/acs.est.8b02219.

Zhi, W., Klingler, C., Liu, J., Li, L., 2023. Widespread deoxygenation in warming rivers. Nat. Clim. Change 13, 1105–1113. https://doi.org/10.1038/s41558-023-01793-3.

Zhou, H.X., Lian, L.S., Yan, S.W., Song, W.H., 2017. Insights into the photo-induced formation of reactive intermediates from effluent organic matter: the role of chemical constituents. Water Res. 112, 120–128. https://doi.org/10.1016/j.watres.2017.01.048.

Zhou, H.X., Yan, S.W., Lian, L.S., Song, W.H., 2019. Triplet-state photochemistry of dissolved organic matter: triplet-state energy distribution and surface electric charge conditions. Environ. Sci. Technol. 53, 2482–2490. https://doi.org/10.1021/acs.est.8b06574.

Zsolnay, A., Baigar, E., Jimenez, M., Steinweg, B., Saccomandi, F., 1999. Differentiating with fluorescence spectroscopy the sources of dissolved organic matter in soils subjected to drying. Chemosphere 38, 45–50. https://doi.org/10.1016/S0045-6535(98)00166-0.